Extended Kalman Filtering for the Modeling and Analysis of ICG Pharmacokinetics in Cancerous Tumors Using NIR Optical Methods

Burak Alacam, *Student Member, IEEE*, Birsen Yazici*, *Senior Member, IEEE*, Xavier Intes, and Britton Chance

***Abstract*—Compartmental modeling of indocyanine green (ICG) pharmacokinetics, as measured by near infrared (NIR) techniques, has the potential to provide diagnostic information for tumor differentiation. In this paper, we present three different compartmental models to model the pharmacokinetics of ICG in cancerous tumors. We introduce a systematic and robust approach to model and analyze ICG pharmacokinetics based on the extended Kalman filtering (EKF) framework. The proposed EKF framework effectively models multiple-compartment and multiple-measurement systems in the presence of measurement noise and uncertainties in model dynamics. It provides simultaneous estimation of pharmacokinetic parameters and ICG concentrations in each compartment. Moreover, the recursive nature of the Kalman filter estimator potentially allows real-time monitoring of time varying pharmacokinetic rates and concentration changes in different compartments. Additionally, we introduce an information theoretic criteria for the best compartmental model order selection, and residual analysis for the statistical validation of the estimates. We tested our approach using the ICG concentration data acquired from four Fischer rats carrying adenocarcinoma tumor cells. Our study indicates that, in addition to the pharmacokinetic rates, the EKF model may provide parameters that may be useful for tumor differentiation.**

***Index Terms*—Compartmental analysis, extended Kalman filter, indocyanine green, pharmacokinetics, tumor characterization.**

I. Introduction

NEAR INFRARED (NIR) diffuse optical imaging and spectroscopy methods provide quantitative functional information that cannot be obtained by the conventional radiological methods [1]–[3]. NIR techniques can provide *in vivo* measurements of the oxygenation and vascularization states, uptake and release of optical contrast agents, and chromophore concentrations with high sensitivity. In particular, NIR diffuse optical techniques in conjunction with optical contrast agents have the potential to characterize angiogenesis, and to differentiate between malignant and benign tumors [4]–[7].

At present, indocyanine green (ICG) is the only NIR optical agent approved for human use. In NIR measurements, the presence of ICG within an imaging volume results in an increased signal that can be observed over the course of the experiment. Study of the time kinetics of ICG concentration curves may provide physiologically relevant information for tumor differentiation. Specifically, cancerous tissue types are expected to show high and fast uptake due to the proliferation of "leaky" angiogenetic microvessels, while normal and fatty tissue show little uptake.

A number of research groups reported compartmental modeling of ICG time-kinetic measurements using NIR methods for tumor diagnosis in animal and human subjects [8]–[10]. A compartmental model is a mathematical description of the concentrations of contrast agents in which each compartment represents a kinetically distinct tissue type. It consists of a set of coupled ordinary differential equations (ODE) and a measurement model. Coefficients of the ODE's are the physiological parameters of interest that represent rates of exchange between different compartments. These parameters are nonlinearly related to the total concentration of ICG measured by NIR methods. Furthermore, concentration of ICG in each compartment cannot be directly measured noninvasively by NIR techniques, making the pharmacokinetic parameter estimation a highly nonlinear problem.

Current methods of ICG compartmental modeling involve curve fitting methods and various techniques for solving differential equations. Gurfinkel *et al.* presented a two-compartment model for ICG kinetics and estimated model parameters [8]. The measurements were obtained using a frequency domain photon migration system coupled with a charge-coupled device. The pharmacokinetic parameters were estimated for each pixel based on a curve fitting method. This study indicated that model parameters show no difference in the ICG uptake rates between normal and diseased tissue. Cuccia *et al.* presented a study of the dynamics of ICG in an adenocarcinoma rat tumor model [9]. A two-compartment model describing the ICG dynamics was used to quantify physiologic parameters related to capillary permeability. The ICG concentration curves were fitted to the compartmental model using a nonlinear least squares Levenberg-Marquart algorithm. It was shown that different tumor types have different capillary permeability rates. Intes *et al.* presented the uptake of ICG by breast tumors using a continuous

Manuscript received April 7, 2005; revised March 10, 2006. This work was supported by U.S. Army Medical Research Acquisition Activity under Grant W81XWH-04-1-0559, in part by the Office of Naval Research under Grant N000014-04-1-0694, and in part by CenSSIS through the Engineering Research Centers Program of National Science Foundation (NSF) under Grant EEC-9986821. The work of X. Intes was supported in part by the National Institute of Health (NIH) under Grant CA110173. *Asterisk indicates corresponding author.*

B. Alacam is with Department of Electrical, Computer, and Systems Engineering, Rensselaer Polytechnic Institute, Troy, NY 12180 USA.

*B. Yazici is with Department of Electrical, Computer, and Systems Engineering, Rensselaer Polytechnic Institute, 110 8th Street, Troy, NY 12180 USA (e-mail: yazici@ecse.rpi.edu).

X. Intes is with Advanced Research Technologies Inc., Saint-Laurent, QC H4S 2A4, Canada.

B. Chance is with Department of Biochemistry and Biophysics, University of Pennsylvania, Philadelphia, PA 16802 USA.

Digital Object Identifier 10.1109/TBME.2006.881796

wave diffuse optical tomography apparatus [10]. A two-compartment model was used to analyze the pharmacokinetics of ICG. A curve fitting algorithm, namely the nonlinear Nelder-Mead simplex search, was used to estimate the pharmacokinetic parameters. This study showed that the malignant cases exhibit slower rate constants (uptake and outflow) as compared to healthy tissue.

While the studies described above demonstrate the feasibility of the ICG pharmacokinetics in tumor characterization; due to the highly nonlinear nature of the pharmacokinetic parameter estimation, variation in parameter values from one subject to another, and sparse data available in clinical and laboratory settings, a *systematic and robust* approach is needed to model, estimate and analyze ICG pharmacokinetics. Such an approach must include: 1) a method for compartmental model order selection; 2) a robust method of estimating ICG pharmacokinetic parameters; 3) a method of validating the selected model and the estimation results.

In this paper, we present three different compartmental models for the ICG pharmacokinetics in cancerous tumors and propose an extended Kalman filtering (EKF) framework to estimate the model parameters. The models capture the transportation of ICG between the vascular and extravascular compartments, including interstitial fluid region, parenchymal cell, intracellular binding site, and extravascular, extracellular spaces (EES). The extended Kalman filter (EKF) is a recursive modeling and estimation method with numerous advantages in ICG pharmacokinetic modeling. These include: 1) effective modeling of multiple compartments, and multiple measurement systems governed by coupled ordinary differential equations, in the presence of measurement noise and uncertainties in the compartmental model dynamics; 2) simultaneous estimation of pharmacokinetic model parameters and ICG concentrations in each compartment, which are not accessible *in vivo* by means of NIR techniques; 3) recursive estimation of time-varying pharmacokinetic model parameters; 4) statistical validation of estimated concentrations and error bounds on the pharmacokinetic parameter estimates; 5) incorporation of available *a priori* information about the initial conditions of the permeability rates into the estimation procedure; 6) potential real-time monitoring of ICG pharmacokinetic parameters and ICG concentrations in different compartments due to the recursive nature of the EKF estimation method. Additionally, we present a method for selecting the optimal compartmental model order based on a Bayesian information criterion, and a statistical validation method based on residual analysis.

We test our approach using the ICG concentration data acquired from four Fisher rats carrying adenocarcinoma tumor cells. Two-, three- and four-compartment models are fitted to data and pharmacokinetic model parameters and concentrations in different compartments are estimated using the EKF framework. The Bayesian information criterion suggests that the two-compartment model provides a sufficient fit for our data. The estimated model order and the model parameters are further validated by residual analysis. The model parameters are used to differentiate between two types of cancerous tumors. Our study suggests that the permeability rates out of the vasculature are higher in edematous tumors as compared to necrotic tumors. Additionally, we observe that in the two-compartment model, the ICG concentration curve is higher in the EES compartment in edematous tumors. This suggests that the ratio of the peak value of the ICG concentrations in different compartments may be a useful parameter to differentiate tumors.

The paper is organized as follows: In Section II, we present the two-, three- and four-compartment models for ICG pharmacokinetics in tissue. In Section III, we present the state-space representation of the compartmental models; estimation of ICG pharmacokinetic parameters and ICG concentrations in the EKF framework; and an optimal model order selection criterion. In Section IV, we present the experimental results obtained from Fischer rat data. Section V summarizes our results and conclusion. Appendix I includes the derivation of the likelihood function used in the Bayesian information criterion.

II. ICG Pharmacokinetic Modeling Using NIR Measurements

A. Indocyanine Green

ICG is an optical dye commonly used in retinopathy and hepatic diagnostics. Given its low toxicity and FDA approval, it has recently been utilized as a blood pooling agent for the detection and diagnosis of cancerous tumors by means of NIR optical methods. The absorption peak of ICG is 805 nm and the fluorescence peak is at 830 nm. ICG has strong affinity for blood proteins. In plasma, ICG is near-completely bound, primarily to albumin. As a result, its *in vivo* kinetics are similar to those of a 70-kD molecule, although it has a molecular weight of about 700 D [11]–[15].

ICG is eliminated from the body primarily through the bile. Outside of the circulatory system, it is not available for removal until it returns to the system. The kinetics of this transition offers a potential means of noninvasively assessing the leakiness of large molecules from the microvasculature; this permeability is a characteristic of the poorly developed vasculature observed in angiogenesis. The increase in local microvasculature density is also expected to induce increased perturbation in the optical signal from intercapillary ICG.

There are some differences in the delivery of ICG between normal and cancerous vasculature. In normal tissue, ICG acts as a blood flow indicator in tight capillaries of normal vessels. However in tumors, ICG may act as a diffusible (extravascular) flow in the leaky capillary of cancer vessels. To investigate the validity of this hypothesis, one has to employ at least a two-compartment model composed of plasma and EES. Additionally, the permeability rate is expected to increase as the malignancy advances [9], [10]. Fig. 1(a) and (b) illustrates the ICG flow for healthy and malignant tissue, respectively.

B. Compartmental Analysis of ICG Pharmacokinetics

Compartmental modeling allows relatively simple and effective mathematical representation of complex biological responses due to contrast agents. A region of interest is assumed to consist of a number of compartments, generally representing a volume or a group of similar tissues into which the contrast agent is distributed. The concentration change in a specific compartment is modeled as a result of the exchange of contrast

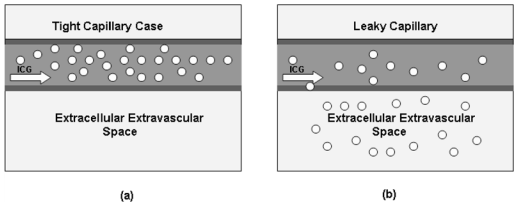

Fig. 1. An illustration of the ICG flow (a) in tight capillary of normal vessel and (b) in permeable capillary of tumor tissue.

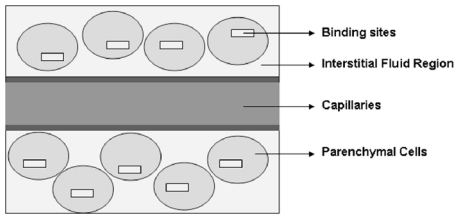

Fig. 2. A simple illustration of the capillary extracapillary structure.

agent between connected compartments. These changes are modeled by a collection of coupled ODEs; each equation describing the time change dictated by the biological laws that govern the concentration exchanges between the interacting compartments [16]–[19]. In this paper, we investigate three different compartmental models for the ICG kinetics and determine the optimal model order based on Bayesian information criteria.

1) Four-Compartment Model: Fig. 2 illustrates the capillary and extracapillary space relevant to the four compartment model. The four-compartment model includes capillary region, interstitial fluid region, parenchymal cell region and intracellular binding site as compartments [20]. The ICG, injected intravenously into the subject, can pass from the capillary into the reversible binding site inside the cell through the interstitial fluid region and the parenchymal cell region [20]–[22]. Moreover, in advanced tumor stages, the leakiness around the tumor vessels is expected to increase, resulting in higher permeability rates during the transportation of ICG into the compartments. A block diagram of the four-compartment transport and chemical model of ICG delivery is shown in Fig. 3(a).

Let $C_p, C_i, C_{\rm pc}$, and C_b denote the ICG concentrations in plasma, the interstitial fluid region, the parenchymal cell region and the intracellular binding site, respectively; and let $k_{\rm out}^{(4)}, k_a^{(4)}, k_b^{(4)}, k_c^{(4)}, k_d^{(4)}, k_e^{(4)}$, and $k_f^{(4)}$ be the constants used as equilibrium coefficients as shown in Fig. 3(a). Then the set of differential equations representing the ICG transition between the four compartments is given as follows.

The leakage into and the drainage out of plasma

$$\frac{dC_p(t)}{dt} = k_b^{(4)} C_i(t) - k_a^{(4)} C_p(t) - k_{out}^{(4)} C_p(t). \quad (1)$$

The leakage into and the drainage out of the interstitial fluid region

$$\frac{dC_i(t)}{dt} = k_a^{(4)} C_p(t) - k_b^{(4)} C_i(t) - k_c^{(4)} C_i(t) + k_d^{(4)} C_{\rm pc}(t). \quad (2)$$

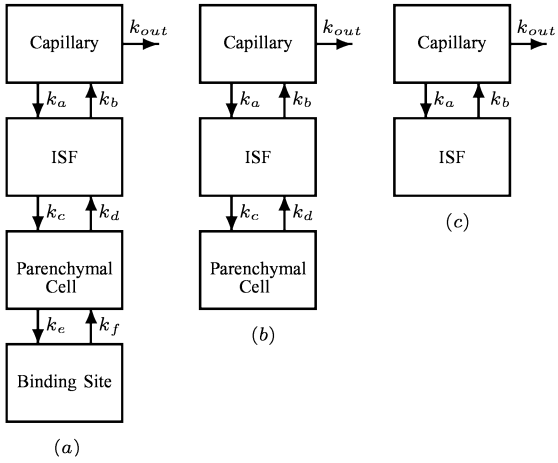

Fig. 3. Block diagrams of the (a) four-compartment, (b) three-compartment, and (c) two-compartment models for the ICG pharmacokinetics.

The leakage into and the drainage out of the parenchymal cell

$$\frac{dC_{\rm pc}(t)}{dt} = k_c^{(4)} C_i(t) - k_d^{(4)} C_{\rm pc}(t) - k_e^{(4)} C_{\rm pc}(t) + k_f^{(4)} C_b(t). \quad (3)$$

The leakage into and the drainage out of the intracellular binding site

$$\frac{dC_b(t)}{dt} = k_e^{(4)} C_{\rm pc}(t) - k_f^{(4)} C_b(t). \quad (4)$$

Physiologically, the equilibrium constants are defined by the permeability surface area products given as $PS\rho$, where P is the capillary permeability constant, S is the capillary surface area, and ρ is the tissue density. $k_{\rm out}^{(4)}$ is proportional to the flow rate into and out of the capillary and $k_a^{(4)}, k_b^{(4)}, k_c^{(4)}, k_d^{(4)}, k_e^{(4)}$, and $k_f^{(4)}$ represent intra-tissue physiologic effects during ICG delivery from the capillary to the binding site. Note that the superscript denotes the order of the compartmental model.

The actual bulk ICG concentration in the tissue measured by NIR spectroscopy, $m(t)$, is a linear combination of the ICG concentrations in the four different compartments

$$m(t) = v_p^{(4)} C_p(t) + v_i^{(4)} C_i(t) + v_{\rm pc}^{(4)} C_{\rm pc}(t) + v_b^{(4)} C_b(t) \quad (5)$$

where $v_p^{(4)}, v_i^{(4)}, v_{\rm pc}^{(4)}$, and $v_b^{(4)}$, are volume fractions of plasma, the interstitial fluid region, the parenchymal cell region and the intracellular binding site, respectively.

2) Three-Compartment Model: In this model, the parenchymal cell and intracellular binding site compartments are combined to form a single compartment called parenchymal cell. This amounts to the assumptions that the transport of ICG into the intracellular binding site is negligible as compared to the other compartments and, therefore, omitted from the model. A block diagram of the three-compartment transport and chemical model of ICG delivery is shown in Fig. 3(b). The three-compartment transport equations are given as follows:

The leakage into and the drainage out of plasma

$$\frac{dC_p(t)}{dt} = k_b^{(3)} C_i(t) - k_a^{(3)} C_p(t) - k_{\text{out}}^{(3)} C_p(t). \quad (6)$$

The leakage into and the drainage out of the interstitial space

$$\frac{dC_i(t)}{dt} = k_a^{(3)} C_p(t) - k_b^{(3)} C_i(t) - k_c^{(3)} C_i(t) + k_d^{(3)} C_{\text{pc}}(t). \quad (7)$$

The leakage into and the drainage out of the parenchymal cell

$$\frac{dC_{\text{pc}}(t)}{dt} = k_c^{(3)} C_i(t) - k_d^{(3)} C_{\text{pc}}(t). \quad (8)$$

The total ICG concentration measured by NIR

$$m(t) = v_p^{(3)} C_p(t) + v_i^{(3)} C_i(t) + v_{\text{pc}}^{(3)} C_{\text{pc}}(t) \quad (9)$$

where $v_p^{(3)}, v_i^{(3)}$, and $v_{\text{pc}}^{(3)}$ and C_p, C_i, and C_{pc} are as defined in the four-compartment model.

3) Two-Compartment Model: In the two-compartment model, the tumor region is assumed to be composed of two compartments, namely the plasma and the extra-cellular extra-vascular space (EES) [9], [23], [24]. The EES is defined as the region that lies outside of both the vascular region and the tumor cells. The transport of the ICG to the third and fourth compartments are assumed to be negligible. Therefore, the last two compartments in the four compartment model is omitted. We consider transcapillary leakage to occur only at the tumor site. We also assume that a small perturbation of the global plasma concentration does not affect the bulk removal. Fig. 3(c) shows the block diagram of the two-compartment model for the ICG kinetics. Let C_p and C_e denote the ICG concentrations in plasma and the EES, respectively. Then the two-compartment ICG chemical transport equations are given as follows.

The leakage into and the drainage out of plasma

$$\frac{dC_p(t)}{dt} = k_b^{(2)} C_e(t) - k_a^{(2)} C_p(t) - k_{\text{out}}^{(2)} C_p(t). \quad (10)$$

The leakage into and the drainage out of the EES

$$\frac{dC_e(t)}{dt} = k_a^{(2)} C_p(t) - k_b^{(2)} C_e(t). \quad (11)$$

The parameters $k_a^{(2)}$ and $k_b^{(2)}$ govern the leakage into and the drainage out of the EES, respectively. The parameter $k_{\text{out}}^{(2)}$ describes the ICG elimination from the body through kidneys and liver.

Actual bulk ICG concentration in the tissue measured by NIR is a linear combination of plasma and EES ICG concentrations given by

$$m(t) = v_p^{(2)} C_p(t) + v_e^{(2)} C_e(t) \quad (12)$$

where the parameters $v_p^{(2)}$ and $v_e^{(2)}$ denote the plasma and EES volume fractions, respectively.

III. Extended Kalman Filtering for the ICG Pharmacokinetics

For the rest of our discussion, we shall use the explicit form of the two-compartment model as a running example to clarify our notation. Note that for the rest of the paper, all matrices and vectors will be in boldface and scalar quantities will be in nonboldface notation.

A. State-Space Representation of the ICG Pharmacokinetics

Coupled differential equations resulting from the two-compartment modeling of the ICG pharmacokinetics can be expressed in state-space representation as follows:

$$\begin{bmatrix} dC_e(t) \\ dC_p(t) \end{bmatrix} = \begin{bmatrix} -k_b^{(2)} & k_a^{(2)} \\ k_b^{(2)} & -(k_a^{(2)} + k_{\text{out}}^{(2)}) \end{bmatrix} \begin{bmatrix} C_e(t) \\ C_p(t) \end{bmatrix} + d\mathbf{B}(t),$$
$$m(t) = \begin{bmatrix} v_e^{(2)} & v_2^{(2)} \end{bmatrix} \begin{bmatrix} C_e(t) \\ C_p(t) \end{bmatrix} + \eta(t) \quad (13)$$

where $d\mathbf{B}(t)$ is the Wiener process increment, $d\mathbf{B}(t) = \boldsymbol{\omega}(t)dt$. Here, $\boldsymbol{\omega}(t)$ and $\eta(t)$ can be thought of as uncorrelated zero-mean Gaussian processes with covariance matrix $\mathbf{Q}$, and variance σ^2, respectively.

In vector-matrix notation, the continuous time state-space representation for the n-compartment model is given by

$$d\mathbf{C}(t) = \boldsymbol{\kappa}(\boldsymbol{\alpha}_n)\mathbf{C}(t)dt + d\mathbf{B}(t)$$
$$m(t) = \mathbf{V}(\boldsymbol{\alpha}_n)\mathbf{C}(t) + \eta(t). \quad (14)$$

In (14), $\mathbf{C}(t)$ denotes the concentration vector; $\boldsymbol{\kappa}(\boldsymbol{\alpha}_n)$ is the system matrix, $\mathbf{V}(\boldsymbol{\alpha}_n)$ is the measurement matrix and $\boldsymbol{\alpha}_n$ is the parameter vector whose elements are the pharmacokinetic constants and the volume fractions for the $n-$compartment model. For example the parameter vector $\boldsymbol{\alpha}_2$ for the two-compartment model is given by

$$\boldsymbol{\alpha}_2 = \begin{bmatrix} k_a^{(2)} & k_b^{(2)} & k_{\text{out}}^{(2)} & v_e^{(2)} & v_p^{(2)} \end{bmatrix}. \quad (15)$$

The ICG measurements in (14) are collected at discrete time instances, $t = kT, k = 0, 1, \ldots$, where T is the sampling period. Therefore, the continuous model described in (14) has to be discretized. To simplify our notation, we shall use $\mathbf{C}(k) = \mathbf{C}(kT)$

and $m(k) = m(kT)$. The discrete state space system and the measurement models are given as follows:

$$\begin{aligned} \mathbf{C}(k+1) &= \boldsymbol{\kappa}_d(\boldsymbol{\alpha}_n)\mathbf{C}(k) + \boldsymbol{\omega}(k) \\ m(k) &= \mathbf{V}_d(\boldsymbol{\alpha}_n)\mathbf{C}(k) + \eta(k) \end{aligned} \tag{16}$$

where $\boldsymbol{\kappa}_d(\boldsymbol{\alpha}_n) = e^{\boldsymbol{\kappa}(\boldsymbol{\alpha}_n)T}$ is the discrete-time system matrix and $V_d(\boldsymbol{\alpha}_n) = V(\boldsymbol{\alpha}_n)$ is the discrete-time measurement matrix. $\boldsymbol{\omega}(k)$ and $\eta(k)$ are zero-mean Gaussian white noise processes with covariance matrix $\mathbf{Q}_d$ and variance σ_d^2, respectively. Discretization of state-space models can be found in various system theory books, see for example [25].

An explicit form of the discrete state space model for the two-compartment case is given as follows:

$$\begin{aligned} \begin{bmatrix} C_e(k+1) \\ C_p(k+1) \end{bmatrix} &= \begin{bmatrix} \tau_{11} & \tau_{12} \\ \tau_{21} & \tau_{22} \end{bmatrix} \begin{bmatrix} C_e(k) \\ C_p(k) \end{bmatrix} + \boldsymbol{\omega}(k) \\ m(k) &= \begin{bmatrix} v_e^{(2)} & v_p^{(2)} \end{bmatrix} \begin{bmatrix} C_e(k) \\ C_p(k) \end{bmatrix} + \eta(k) \end{aligned} \tag{17}$$

where τ_{ij} is the ith row and jth column entry of the system matrix $\boldsymbol{\kappa}_d(\boldsymbol{\alpha}_2)$. Note that the matrix entry τ_{ij} is an exponential function of the parameters $k_a^{(2)}, k_b^{(2)}$, and $k_{\text{out}}^{(2)}$.

To simplify the estimation process, we shall first estimate the matrix entries, τ_{ij}, of the discrete-time system matrix $\boldsymbol{\kappa}_d(\boldsymbol{\alpha}_n)$ and then compute the pharmacokinetic parameters for each compartmental model.

B. Modeling of ICG Pharmacokinetic Parameters and Concentrations in an Extended Kalman Filter Framework

The Kalman filter provides a recursive method to estimate the states in state-space models, in which the states are driven by noise, and the measurements are collected in the presence of measurement noise [26]–[28]. In the case of nonlinear state-space models, the extended Kalman filter linearizes the model around the current state estimate, and then applies the KF to the resulting linear model. The EKF framework is also utilized for the joint estimation of the unknown system and/or measurement parameters and states. In a linear state-space model when both states and system parameters are unknown, the linear state-space model can be regarded as a nonlinear model in which the linear system parameters and states are combined to form the new states of the nonlinear model. This system is then linearized and solved for the unknown states using the KF estimator. We consider a linear Taylor approximation of the nonlinear model. The details of the linearization procedure and a general discussion on EKF can be found in [27] and [29]–[31].

In our problem, the objective is to simultaneously estimate the states, i.e., the ICG concentrations in each compartment, and the system and measurement parameters, i.e., the pharmacokinetic parameters and the volume fractions. Let $\boldsymbol{\theta}_n$ denote the discrete-time parameter vector of the pharmacokinetic rates and volume fractions. For example, in the two-compartment model, $\boldsymbol{\theta}_2$ is given by

$$\boldsymbol{\theta}_2 = \begin{bmatrix} \tau_{11} & \tau_{12} & \tau_{21} & \tau_{22} & v_e^{(2)} & v_p^{(2)} \end{bmatrix}^T. \tag{18}$$

Note that the parameter vector $\boldsymbol{\theta}_n$, derived from the state space model (17), is time independent. In order to estimate $\boldsymbol{\theta}_n$ within the EKF framework, the following dynamic model is introduced:

$$\boldsymbol{\theta}_n(k+1) = \boldsymbol{\theta}_n(k) + \boldsymbol{\varsigma}(k) \tag{19}$$

where $\boldsymbol{\varsigma}(k)$ is a zero-mean white noise process with covariance matrix $\mathbf{S}_d$ [27]. Here, $\boldsymbol{\theta}_n(k)$ can be thought of as the kth update of the parameter rather than its value at time k.

We append the parameter vector $\boldsymbol{\theta}_n(k+1)$ to the ICG concentration vector $\mathbf{C}(k+1)$ to form the new nonlinear state-space model given by

$$\begin{aligned} \begin{bmatrix} \mathbf{C}(k+1) \\ \boldsymbol{\theta}_n(k+1) \end{bmatrix} &= \begin{bmatrix} \mathbf{K}(\boldsymbol{\theta}_n)\mathbf{C}(k) \\ \boldsymbol{\theta}_n(k) \end{bmatrix} + \begin{bmatrix} \boldsymbol{\omega}(k) \\ \boldsymbol{\varsigma}(k) \end{bmatrix} \\ m(k) &= \begin{bmatrix} \mathbf{V}_d(\boldsymbol{\theta}_n) & 0 \end{bmatrix} \begin{bmatrix} \mathbf{C}(k) \\ \boldsymbol{\theta}_n(k) \end{bmatrix} + \eta(k) \end{aligned} \tag{20}$$

where $\mathbf{K}(\theta_n) = \boldsymbol{\kappa}_d(\boldsymbol{\alpha}_n)$.

C. EKF Joint Estimation of ICG Concentrations, Pharmacokinetic Parameters, and Volume Fractions

In this section, we will summarize the major steps of the EKF estimator for the joint estimation of ICG concentrations and compartmental model parameters.

Let the subscript $k \mid t$ denote the estimate at time k given all the measurements up to time t. Then the 1-step ahead prediction of the ICG concentrations and the compartmental model parameters are given as follows:

$$\begin{bmatrix} \hat{\mathbf{C}} \\ \hat{\boldsymbol{\theta}_n} \end{bmatrix}_{k \mid k-1} = \begin{bmatrix} \mathbf{K}(\hat{\boldsymbol{\theta}_n})\hat{\mathbf{C}} \\ \hat{\boldsymbol{\theta}_n} \end{bmatrix}_{k-1 \mid k-1}. \tag{21}$$

For the two-compartment model, (21) becomes

$$\begin{bmatrix} \hat{C_e} \\ \hat{C_p} \\ \hat{\boldsymbol{\theta}_2} \end{bmatrix}_{k \mid k-1} = \begin{bmatrix} \hat{\tau_{11}}\hat{C_e} + \hat{\tau_{12}}\hat{C_p} \\ \hat{\tau_{21}}\hat{C_e} + \hat{\tau_{22}}\hat{C_p} \\ \hat{\boldsymbol{\theta}_2} \end{bmatrix}_{k-1 \mid k-1}. \tag{22}$$

The error covariance matrix, $\mathbf{P}_{k \mid k-1}$, of the 1-step ahead predictions is given as follows:

$$\mathbf{P}_{k \mid k-1} = \mathbf{J}_{k-1}\mathbf{P}_{k-1 \mid k-1}\mathbf{J}_{k-1}^T + \begin{bmatrix} \mathbf{Q}_d & 0 \\ 0 & \mathbf{S}_d \end{bmatrix} \tag{23}$$

where $\mathbf{J}_k$ is the Jacobian of the nonlinear EKF system function at time k. Explicitly, it is given by:

$$\mathbf{J}_k = \begin{bmatrix} \mathbf{K}(\hat{\boldsymbol{\theta}}_n) & \frac{\partial}{\partial \boldsymbol{\theta}_n}[\mathbf{K}(\hat{\boldsymbol{\theta}}_n)\hat{\mathbf{C}}] \\ \mathbf{0} & \mathbf{I} \end{bmatrix}_{k\,|\,k} \tag{24}$$

where $\mathbf{0}$ and $\mathbf{I}$ denote zero and identity matrices, respectively. The Jacobian matrix for the two-compartment model becomes

$$\mathbf{J}_k = \begin{bmatrix} \begin{pmatrix} \hat{\tau_{11}} & \hat{\tau_{12}} \\ \hat{\tau_{21}} & \hat{\tau_{22}} \end{pmatrix} & \begin{pmatrix} \hat{C_e} & \hat{C_p} & 0 & 0 & 0 & 0 \\ 0 & 0 & \hat{C_e} & \hat{C_p} & 0 & 0 \end{pmatrix} \\ \mathbf{0}_{(6\times 2)} & \mathbf{I}_{(6\times 6)} \end{bmatrix}_{k\,|\,k} \tag{25}$$

where $\mathbf{0}_{(6\times 2)}$ is a 6×2 zero matrix, and $\mathbf{I}_{(6\times 6)}$ is a 6×6 identity matrix.

The 1-step ahead predictions are updated to the kth-step estimates by means of the Kalman gain matrix which is given by

$$\mathbf{G}_k = \mathbf{P}_{k\,|\,k-1}\boldsymbol{\Lambda}^T \left[\boldsymbol{\Lambda}\mathbf{P}_{k\,|\,k-1}\boldsymbol{\Lambda}^T + \sigma_k^2\right]^{-1} \tag{26}$$

where $\boldsymbol{\Lambda}$ is the following vector:

$$\left[\mathbf{V}_d(\hat{\boldsymbol{\theta}}) \quad \frac{\partial}{\partial \boldsymbol{\theta}}[\mathbf{V}_d(\hat{\boldsymbol{\theta}})\hat{\mathbf{C}}]\right]_{k\,|\,k-1}. \tag{27}$$

For the two-compartment model the $\boldsymbol{\Lambda}$ vector becomes

$$\left[\hat{v_e}^{(2)} \quad \hat{v_p}^{(2)} \quad 0 \quad 0 \quad 0 \quad 0 \quad \hat{C_e} \quad \hat{C_p}\right]_{k\,|\,k-1}. \tag{28}$$

The kth-step estimate of the concentrations and the parameters are obtained recursively using

$$\begin{bmatrix} \hat{\mathbf{C}} \\ \hat{\boldsymbol{\theta}} \end{bmatrix}_{k\,|\,k} = \begin{bmatrix} \hat{\mathbf{C}} \\ \hat{\boldsymbol{\theta}} \end{bmatrix}_{k\,|\,k-1} + \mathbf{G}_k(m(k) - [\mathbf{V}_d(\hat{\boldsymbol{\theta}})\hat{\mathbf{C}}]_{k\,|\,k-1}). \tag{29}$$

For the two-compartment case, the kth-step estimate of the concentrations and the parameters is

$$\begin{bmatrix} \hat{C_e} \\ \hat{C_p} \\ \hat{\boldsymbol{\theta}}_2 \end{bmatrix}_{k\,|\,k} = \begin{bmatrix} \hat{C_e} \\ \hat{C_p} \\ \hat{\boldsymbol{\theta}}_2 \end{bmatrix}_{k\,|\,k-1} + \mathbf{G}_k \left[m(k) - \left(\hat{v_e}^{(2)}\hat{C_e} - \hat{v_p}^{(2)}\hat{C_p}\right)_{k\,|\,k-1}\right]. \tag{30}$$

The error covariance matrix, $\mathbf{P}_{k\,|\,k}$, of the kth-step estimates is updated as

$$\mathbf{P}_{k\,|\,k} = [\mathbf{I} - \mathbf{G}_k\boldsymbol{\Lambda}]\mathbf{P}_{k\,|\,k-1} \tag{31}$$

where $\mathbf{I}$ is the identity matrix.

In general, the convergence of EKF depends on proper choices of the initial values of the parameters, $\boldsymbol{\theta}$, initial values of the concentrations, $\mathbf{C}$, and proper selection of the noise covariance matrices $\mathbf{S}_d, \mathbf{Q}_d$, and the variance σ_d^2 [33]. The parameter σ_d^2 controls the convergence of the Kalman gain $\mathbf{G}_k$. To ensure stability, we set σ_d^2 much higher than the $\boldsymbol{\Lambda}P_{k\,|\,k-1}\boldsymbol{\Lambda}^T$ term in (26). However, setting very high values of σ_d^2 leads to slow convergence of the Kalman gain $\mathbf{G}_k$. The main cause of divergence in EKF can be tracked down to the fact that a change in the parameter vector has no direct effect on the Kalman gain; in other words, there is no coupling term between the Kalman gain and the parameter vector [34]. Based on this observation, we improved the convergence of the EKF by modifying the term $\mathbf{J}(1,2) = (\partial/\partial\boldsymbol{\theta})\mathbf{K}(\hat{\boldsymbol{\theta}})\hat{\mathbf{C}}$ in (24), as described in [34].

It has been shown that if $\mathbf{Q}_d, \mathbf{S}_d$, and σ_d^2 are selected less than the actual values, it leads to overconfidence in the accuracy of the estimates of the error covariance matrix [32]. Therefore, we regarded these matrices as tuning parameters and not as the estimates of the true covariance matrices, as suggested in [32].

Theoretically, the state estimates can be initialized at the expected value of the ICG concentrations, i.e., $E[\mathbf{C}(0)]$. One approach to the initialization of the parameters is to utilize the state-space presentation given in (16). Since $E(m(0)) = \mathbf{V}_d(\boldsymbol{\theta}_n(0))E[\mathbf{C}(0)], m(0) - \mathbf{V}_d(\boldsymbol{\theta}_n(0))E[\mathbf{C}(0)]$ is a zero-mean random variable. If we express the variance of the measurement $m(0)$ in terms of the variance of $\mathbf{C}(0)$ using the measurement model in (16), and solve for $\boldsymbol{\theta}_n$, we get the estimate $\hat{\boldsymbol{\theta}}_n(0)$ as the most appropriate value for initialization. The details of the selection of the initial values for the parameters can be found in [27].

The initialization of the error covariance matrix is also important for the performance of the EKF. The error covariance matrix is the matrix which provides information about the error bounds for the estimates. Theoretically, the initial error covariance matrix is a diagonal matrix where the diagonal entries are the initial estimates of the variance of concentrations and pharmacokinetic parameters, i.e.,

$$\mathbf{P}_{0\,|\,0} = \begin{bmatrix} \mathrm{Cov}(\mathbf{C}(0)) & 0 \\ 0 & \mathbf{S}_d \end{bmatrix}. \tag{32}$$

In depth discussion on the convergence properties of the EKF can be found in [27] and [32]–[34].

D. Compartmental Model Order Selection

We adopted the Bayesian information criterion (BIC) for the optimal model order selection. BIC is a well known information theoretic criterion, in which the optimal model order is selected by minimizing a cost function to avoid overfitting. The cost function depends on the number of observations, the number of unknown parameters to be estimated and the likelihood function. A detailed discussion of the BIC can be found in [35]–[37].

In order to calculate the BIC for different compartmental models, we first derived a likelihood function for the extended Kalman filter. The derivation is based on maximum likelihood estimation of the parameters in the Kalman filtering framework given as in [38] and [39]. We then modified this likelihood function for the extended Kalman filter estimator for the joint estimation of compartmental model parameters and concentrations. The details of the derivation is provided in the Appendix I.

TABLE I
FOUR-COMPARTMENT MODEL: ESTIMATED PHARMACOKINETIC PARAMETERS USING EKF ALGORITHM

	$k_a^{(4)}$ $(sec^{-1}10^{-2})$	$k_b^{(4)}$ $(sec^{-1}10^{-2})$	$k_c^{(4)}$ $(sec^{-1}10^{-2})$	$k_d^{(4)}$ $(sec^{-1}10^{-2})$	$k_e^{(4)}$ $(sec^{-1}10^{-2})$	$k_f^{(4)}$ $(sec^{-1}10^{-2})$	$k_{out}^{(4)}$ $(sec^{-1}10^{-3})$
Rat 1 (Necrotic)	1.45±0.013	1.22±0.019	1.86±0.017	2.02±0.026	2.74±0.041	2.41±0.051	4.05±0.059
Rat 2 (Necrotic)	3.48±0.048	2.77±0.034	4.28±0.048	4.33±0.040	2.98±0.048	3.03±0.061	4.76±0.062
Rat 3 (Edematous)	4.94±0.052	5.16±0.067	4.22±0.052	4.13±0.067	4.14±0.070	4.27±0.078	5.39±0.085
Rat 4 (Edematous)	5.25±0.053	5.31±0.063	5.07±0.068	5.22±0.063	4.43±0.075	4.03±0.072	3.85±0.056

TABLE II
THREE-COMPARTMENT MODEL: ESTIMATED PHARMACOKINETIC PARAMETERS USING EKF ALGORITHM

	$k_a^{(3)}$ $(sec^{-1}10^{-2})$	$k_b^{(3)}$ $(sec^{-1}10^{-2})$	$k_c^{(3)}$ $(sec^{-1}10^{-2})$	$k_d^{(3)}$ $(sec^{-1}10^{-2})$	$k_{out}^{(3)}$ $(sec^{-1}10^{-3})$
Rat 1 (Necrotic)	1.93±0.061	1.28±0.049	1.82±0.032	2.02±0.041	3.89±0.052
Rat 2 (Necrotic)	4.41±0.074	2.48±0.067	4.87±0.066	5.03±0.057	5.45±0.071
Rat 3 (Edematous)	4.71±0.085	3.88±0.077	4.95±0.059	4.68±0.050	4.42±0.040
Rat 4 (Edematous)	5.29±0.091	6.48±0.096	4.48±0.062	4.20±0.048	5.01±0.055

IV. EXPERIMENTAL RESULTS—ICG PHARMACOKINETICS IN FISCHER RAT DATA

We applied the proposed EKF framework to the pharmacokinetic analysis of ICG data obtained from four Fischer rats with adenocarcinoma. R3230ac adenocarcinoma cells were injected below the skin into four Fischer rats three weeks prior to measurements. The tumor size for the rats varies in diameter from 5 to 30 mm. Measurements were conducted with a combined frequency-domain and steady-state optical technique that facilitates rapid measurement of tissue absorption. Frequency domain measurements were obtained at 674, 800, 849, 898, and 915 nm, modulated at frequencies from 50 to 601 MHz, sweeping a total of 233 frequencies. Tumors were also imaged by use of contrast-enhanced magnetic resonance imaging and coregistered with the location of the optical probe. In addition, a broadband continuous wave reflectance measurement spanning the range 650–1000 nm was performed with a spectrometer. With the reduced-scattering coefficient spectrum and diffusion theory, the broadband reflectance spectra were converted to absorption coefficient spectra. The absolute concentration of ICG, together with oxy-hemoglobin, deoxy-hemoglobin, and water were calculated by using multiple linear regressions of ICG extinction coefficient spectra to the calculated absorption spectrum at approximately every second for 10 min. A detailed discussion of the measurement process and apparatus can be found in [40] and [41].

Fig. 4 presents the ICG concentrations (μM) from four different rats. Tumors in Rat 1 and 2 are classified as necrotic because of their low tissue oxy-hemoglobin, low total hemoglobin, and low gadolinium-diethylene-triamine penta-acetic acid (Gd-DTPA) enhancement levels. Tumors in Rat 3 and 4 are classified as edematous due to their high water content [42]. It can be observed from Fig. 4 that the necrotic cases display low peak ICG concentration values and slowly rising slopes unlike the edematous cases with high peak values and sharp rising slopes.

We estimated the pharmacokinetic rates for the four-, three- and two-compartment models. Each data set has 504 measurements. The reported parameter estimates are the asymptotic values obtained when the extended Kalman filter has converged.

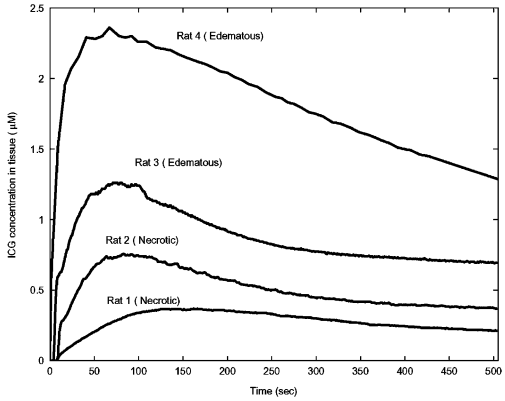

Fig. 4. ICG concentrations measured in tissue for four different rats.

In other words, the predicted parameter values corresponding to the final estimate, i.e., $k_a^2 = k_{a,(k=504)}^2$. The results are given in Tables I, II, and III, respectively. The error bounds on the estimates are derived from the covariance matrix of the EKF estimator. The estimated pharmacokinetic rates for all compartmental models indicate that the exchange rates between the capillary and the adjacent compartment (ISS or EES), $k_a^n, k_b^n,\ n = 2,3,4$, are significantly different for the necrotic and edematous tissue. We observe that for the four- and three-compartment models, the estimated exchange rates between the ISS and parenchymal cell compartments, $k_c^n, k_d^n,\ n = 3,4$, are comparable. Similarly, the estimated rate of drainage out of the plasma, $k_{\text{out}}^n,\ n = 2,3,4$, are consistent for all models.

Based on the model parameter estimates, we computed the BIC values for each rat data to reveal overfitting. The BIC values and the number of unknown parameters for each rat data are tabulated in Table IV. The BIC suggests that the two-compartment model is sufficient for all four measurement sets.

We further analyze the goodness-of-fit of the compartmental models by means of residual analysis. The basic idea of residual analysis is to compare the actual measurements $m(k)$ with their 1-step ahead predictions, $\hat{m}(k)_{k\,|\,k-1}$, based on the estimated

TABLE III
TWO-COMPARTMENT MODEL: ESTIMATED PHARMACOKINETIC PARAMETERS AND VOLUME FRACTIONS USING EKF ALGORITHM

	$k_a^{(2)}$ $(sec^{-1}10^{-2})$	$k_b^{(2)}$ $(sec^{-1}10^{-2})$	$k_{out}^{(2)}$ $(sec^{-1}10^{-3})$	$v_e^{(2)}$ (10^{-2})	$v_p^{(2)}$ (10^{-2})
Rat 1 (Necrotic)	2.47±0.043	1.06±0.052	4.61±0.073	21.8±1.92	1.41±0.053
Rat 2 (Necrotic)	3.54±0.082	2.98±0.086	4.83±0.092	25.4±3.49	2.42±0.088
Rat 3 (Edematous)	6.90±0.101	4.93±0.072	3.95±0.048	30.4±2.81	4.84±0.120
Rat 4 (Edematous)	8.40±0.114	7.77±0.091	4.02±0.068	53.0±4.73	7.03±0.321

TABLE IV
TEST FOR MODEL ORDER SELECTION FOR THREE DIFFERENT COMPARTMENTAL MODELS FOR FOUR DIFFERENT DATA SETS

		Rat1	**Rat2**	**Rat3**	**Rat4**
Model	p	$\phi_{BIC}(p)$	$\phi_{BIC}(p)$	$\phi_{BIC}(p)$	$\phi_{BIC}(p)$
Two-comp. Model	7	-178.24	-198.36	-202.81	-172.09
Three-comp. Model	11	-71.62	-83.85	-92.18	-63.91
Four-comp. Model	15	-39.72	-45.12	-56.34	-30.02

TABLE V
THE MEAN AND VARIANCE OF THE ERROR BETWEEN THE ESTIMATES AND MEASUREMENTS

	Four-compartment		**Three-compartment**		**Two-compartment**	
	Mean	Variance	Mean	Variance	Mean	Variance
Rat1	0.0987	7.6e-004	0.0605	4.7e-004	0.0072	2.5e-005
Rat2	0.1043	9.1e-004	0.0767	3.0e-004	0.0057	4.8e-005
Rat3	0.1204	8.9e-004	0.0883	4.9e-004	0.0041	3.0e-005
Rat4	0.0904	5.9e-004	0.0589	6.8e-004	0.0076	8.6e-005

TABLE VI
SNR VALUES FOR THREE DIFFERENT COMPARTMENTAL MODELS FOR FOUR DIFFERENT DATA SETS

	Rat1	**Rat2**	**Rat3**	**Rat4**
Model	SNR (dB)	SNR	SNR	SNR
Two-compartment Model	73.2	68.1	108.3	107.9
Three-compartment Model	30.7	36.1	23.9	47.0
Four-compartment Model	20.8	29.9	27.7	18.4

parameters. A detailed discussion on residual analysis can be found in [26] and [43]. The mean and variance of the residual error for the four-, three- and two-compartmental models are tabulated in Table V. To normalize the error with respect to the magnitude of the actual measurements, we calculated the signal-to-noise ratio (SNR) using the median value of the measurements and the mean of the residual errors for each rat data. As seen from the results in Table VI, the SNR values are higher for the two-compartment case for all data sets. These results show that the two-compartment model provides the minimum bias and the best statistical efficiency. Fig. 5 shows the measured total concentration data and its 1-step ahead prediction based on the two-compartment model for each rat data. Clearly, there is a good agreement between the actual and the predicted values.

Based on the BIC and residual analysis, we conclude that the two-compartment model provides the best statistical fit for the rat data and investigate the estimated model parameters in more detail.

In the two-compartment model, the rate of leakage into the EES from the capillary, $k_a^{(2)}$, range from 0.0247 to 0.0840 s^{-1}

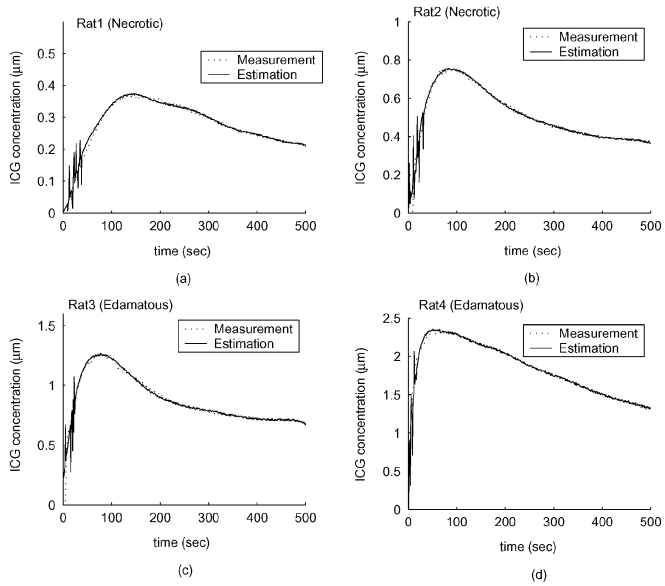

Fig. 5. ICG concentration measurement data and 1-step prediction of the measurements for four different rats.

and the rate of drainage out of the EES and into the capillary, $k_b^{(2)}$, range from 0.0106 to 0.0777 s^{-1}. Note that the permeability rates for the necrotic cases are lower than the ones observed for the edematous cases. Additionally, the estimated values for the pharmacokinetic rates are much higher than the normal tissue values due to the increased leakiness of the blood vessels around the tumor region [9], [44]. The estimated plasma volume fractions agrees with the values reported earlier [9], and the values presented in the literature [45], [46]. These results confirm that $v_p^{(2)}$ can be large in tumors and that its magnitude varies with respect to the stage of the tumor [24]. The estimated values of the EES volume fraction, $v_e^{(2)}$, range from 0.218 to 0.53, in agreement with the 0.2 to 0.5 range reported earlier [23]. Note that these results are valid only for the ICG pharmacokinetics in tumor cells R3230ac, adenocarcinoma and may not be generalized for other types of contrast agents or tumor types.

Fig. 6 shows the estimated ICG concentrations in plasma and the EES compartments for the two-compartment model for Rats 1 to 4. Note that the concentration curves in Figs. 5 and 6 follow a similar time course since the curves in Fig. 6 is a linear combination of the curves in Fig. 5. Note that initial estimates of concentrations are noisy due to the limited data used in the recursive EKF estimation. This can be improved by Kalman backward smoothing [47]. The peak values of the plasma concentration, C_p, range from 2.72 μM to 4.28 μM. The absolute value of the concentrations may not be very useful. However, concentration

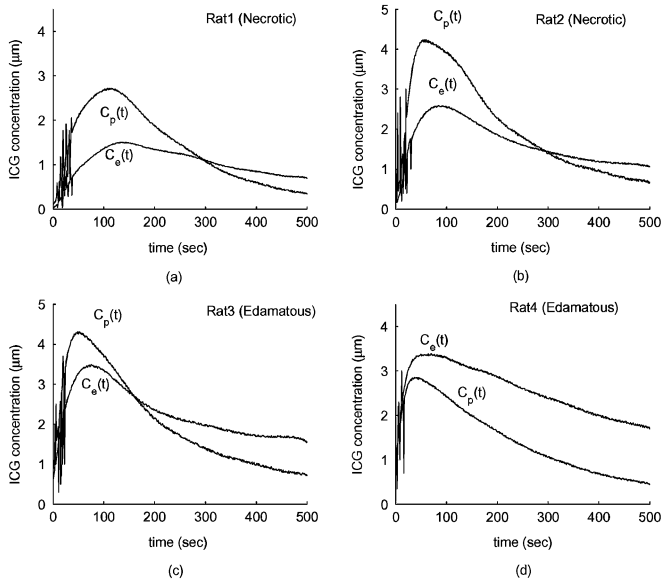

Fig. 6. ICG concentrations in plasma, $C_p(t)$ and EES, $C_e(t)$, for four different rats. (a) Rat1, (b) Rat2, (c) Rat3, and (d) Rat4.

of ICG in a compartment relative to the one in another compartment may provide useful information. We consider the ratio of the peak concentrations in plasma and the EES as a potential parameter to discriminate different tumors. The peak C_p/C_e ratio for Rats 1 to 4 is 0.551, 0.593, 0.787, 1.151, respectively. This ratio is higher in edematous cases consistent with the fact that ICG-albumin leaks more into the EES in edematous tumors. Additionally, the ICG concentration in plasma decays faster than the ICG concentration in the EES due to its elimination through the liver and kidneys.

V. Conclusion

In this paper we present three different compartmental models, an extended Kalman filtering framework for the modeling, and estimation of ICG pharmacokinetics in cancerous tumors based on NIR measurements. Additionally, we introduce an information theoretic criterion and residual analysis for model selection and statistical validation. The proposed compartmental models are fit to data obtained from Fischer rats with adenocarcinoma cells. The pharmacokinetic rates and volume fractions are estimated for all models. The estimated rates for all compartmental models indicate that the exchange rates between the capillary and the adjacent compartment (ISS or EES) are significantly larger for the edematous tissue as compared to the necrotic cases. Based on the BIC and residual analysis, we conclude that the two-compartment model provides the best statistical fit for the rat data and ICG pharmacokinetics. Parameters of this model indicate that the permeability rates are higher for edematous cases as compared to the necrotic tumors. Additionally, we estimated the ICG concentrations in different compartments. The concentrations in different compartments may provide additional parameters for tissue characterization.

While our study indicates that the two-compartment model provides the best fit for the ICG pharmacokinetics, the three- or four-compartment models may be advantageous for modeling the pharmacokinetics of functionalized optical contrast agents that actively accumulate or activate in diseased tissue [48]–[50]. In the near future, we plan to analyze the pharmacokinetics of optical agents within the framework of EKF using data sets collected from animals and human subjects.

Appendix

The cost function for the BIC is given by

$$\phi_{\mathrm{BIC}}(p) = p\ln N - 2\ln L(\boldsymbol{\theta}_p, m(1), \ldots, m(N)) \tag{33}$$

where p is the dimension of $\boldsymbol{\theta}_p$, which is related to the number of compartments in the model, N is the data length, and $L(\boldsymbol{\theta}, m(1), m(2), \ldots, m(N))$ is the likelihood function. The likelihood function for the EKF is given by

$$L(mbi\theta, m(1), \ldots, m(N)) = -\frac{1}{2}\sum_{k=1}^{N}\ln[\det(\mathbf{H}_k)] - \frac{1}{2}\sum_{k=1}^{N}\mathbf{A}_k^T\mathbf{H}_k^{-1}\mathbf{A}_k \tag{34}$$

where the matrix $\mathbf{H}$ is defined as

$$\mathbf{H}_k = \Lambda\mathbf{P}_{k\,|\,k-1}\mathbf{\Lambda}^T + \sigma_k^2 \tag{35}$$

and $\sigma_k^2, \mathbf{\Lambda}$, and $\mathbf{P}_{k\,|\,k-1}$ are as defined in Section III-C. The vector $\mathbf{A}$ is defined as

$$\mathbf{A}_k = m(k) - [V_d(\hat{\boldsymbol{\theta}})\hat{\mathbf{C}}]_{k\,|\,k-1} \tag{36}$$

where $m(k)$ is the ICG concentration data collected from Fisher rats at time k, and $[\mathbf{V}_d(\hat{\boldsymbol{\theta}})\hat{\mathbf{C}}]_{k\,|\,k-1}$ is the 1-step ahead estimate of the volume fractions and concentrations. The explicit form of the likelihood function for BIC calculation is given by

$$\begin{aligned} &L(\boldsymbol{\theta}, m(1), \ldots, m(N)) \\ &\quad = -\frac{1}{2}\sum_{k=1}^{N}\ln\left[\det\left(\mathbf{\Lambda}\mathbf{P}_{k\,|\,k-1}\mathbf{\Lambda}^T + \sigma_k^2\right)\right] \\ &\qquad -\frac{1}{2}\sum_{k=1}^{N}[m(k) - [\mathbf{V}_d(\hat{\boldsymbol{\theta}})\hat{\mathbf{C}}]_{k\,|\,k-1}]^T \\ &\qquad \times \left[\mathbf{\Lambda}\mathbf{P}_{k\,|\,k-1}\mathbf{\Lambda}^T + \sigma_k^2\right]^{-1} \\ &\qquad \cdot [m(k) - [\mathbf{V}_d(\hat{\boldsymbol{\theta}})\hat{\mathbf{C}}]_{k\,|\,k-1}]. \end{aligned} \tag{37}$$

where all the parameters and matrices are as defined in Section III-C.

Acknowledgment

The authors would like to thank Dr. B. Tromberg and D. Cuccia for providing the rat data used in our study.

References

[1] A. Yodh and B. Chance, "Spectroscopy and imaging with diffusing light," *Phys. Today*, vol. 48-3, pp. 34–40, 1995.
[2] X. Intes and B. Chance, "Non-PET functional imaging techniques: Optical," *Radiol. Clin. N Am.*, vol. 43, pp. 221–234, 2005.

[3] D. Boas, D. Brooks, E. Miler, C. DiMarzio, M. Kilmer, and R. Gaudette, "Imaging the body with diffuse optical tomography," *IEEE Signal Process. Mag.*, vol. 18, no. 6, pp. 57–74, Nov. 2001.

[4] D. Hawrys and E. Sevick-Muraca, "Developments toward diagnostic breast cancer imaging using Near-Infrared optical measurements and fluorescent contrast agents," *Neoplasia*, vol. 2, pp. 388–417, 2000.

[5] K. Furukawa, D. H. Crean, T. S. Mang, H. Kato, and T. J. Dougherty, "Fluorescence detection of premalignant, malignant, and micrometastatic disease using hexylpyropheophorbide," *Proc. SPIE*, vol. 2371, pp. 510–514, 1995.

[6] Y. Chen, Q. Liu, P. Huang, S. Hyman, X. Intes, W. Lee, and B. Chance, "Assessment of tumor angiogenesis using fluorescence contrast agents," *Proc. SPIE*, vol. 5254, no. 1, pp. 296–301, 2003.

[7] A. Becker, G. Schneider, B. Riefke, K. Licha, and W. Semmler, "Localization of near-infrared contrast agents in tumors by intravital microscopy," *Proc. SPIE*, vol. 3568, pp. 112–118, 1999.

[8] M. Gurfinkel, A. B. Thompson, W. Ralston, T. L. Troy, A. L. Moore, T. A. Moore, J. D. Gust, D. Tatman, J. S. Reynolds, B. Muggenburg, K. Nikula, R. Pandey, R. H. Mayer, D. J. Hawrysz, and E. M. Sevick-Muraca, "Pharmacokinetics of ICG and HPPH-car for the detection of normal and tumor tissue using fluorescence, near-infrared reflectance imaging: A case study," *Photochem. Photobiol.*, vol. 72, pp. 94–102, 2000.

[9] D. J. Cuccia, F. Bevilacqua, A. J. Durkin, S. Merritt, B. J. Tromberg, G. Gulsen, H. Yu, J. Wang, and O. Nalcioglu, "*In vivo* quantification of optical contrast agent dynamics in rat tumors by use of diffuse optical spectroscopy with magnetic resonance imaging coregistration," *Appl. Opt.*, vol. 42, no. 1, pp. 2940–2950, June 2003.

[10] X. Intes, J. Ripoll, Y. Chen, S. Nioka, A. G. Yodh, and B. Chance, "*In vivo* continuous-wave optical breast imaging enhanced with Indocyanine Green," *Med. Phys.*, vol. 30-6, pp. 1039–1047, Jun. 2003.

[11] D. Hansen, A. Spence, T. Carski, and M. Berger, "Indocyanine green (ICG) staining and demarcation of tumor margins in a rat glioma model," *Surg. Neurol.*, vol. 40, pp. 451–456, 1993.

[12] H. Shinohara, A. Tanaka, T. Kitai, N. Yanabu, T. Inomoto, S. Satoh, Hatano, Y. Yamaoka, and K. Hirao, "Direct measurement of hepatic Indocyanine Green clearance with near-infrared spectroscopy: Separate evaluation of uptake and removal," *Hepatology*, vol. 23, pp. 137–144, 1996.

[13] A. ElDeosky, A. Seifalian, M. Cope, D. Delpy, and B. Davidson, "Experimental study of liver dysfunction evaluated by direct Indocyanine green clearance using near infrared spectroscopy," *Br. J. Surg.*, vol. 86, pp. 1005–1011, 1999.

[14] X. Li, B. Beauvoit, R. White, S. Nioka, B. Chance, and A. Yodh, "Tumor localization using fluorescence of Indocyanine Green (ICG) in rat models," *Proc. SPIE*, vol. 2389, pp. 789–797, 1995.

[15] M. S. Yates, C. J. Bowmer, and J. Emmerson, "The plasma clearance of indocyanine green in rats with acute renal failure: Effect of dose and route of administration," *Biochem. Pharmacol.*, vol. 32, pp. 3109–3114, 1983.

[16] C. W. Tornoe, "Grey-Box PK/PD Modeling of Insulin," M.S. thesis, Tech. Univ. Denmark, Lyngby, Denmark, Jun. 28, 2002.

[17] D. H. Anderson, *Lecture Notes in Biomathematics: Compartmental Modeling and Tracer Kinetics*. Berlin, Germany: Springer-Verlag, 1983.

[18] J. A. Jacquez, *Compartmental Analysis in Biology and Medicine: Kinetics of Distribution of Tracer-Labeled Materials*. New York: Elsevier, 1972.

[19] C. Cobelli, D. Foster, and G. Toffolo, *Tracer Kinetics in Biomedical Research: From Data to Model*. New York: Kluwer Academic/Plenum, 2000.

[20] P. Huang, X. Intes, B. Chance, and S. Nioka, "Simulation of delivery of indocynanine green injected intravenously into the human subject for breast cancer detection," *Proc. SPIE*, vol. 4949, pp. 450–459, 2003.

[21] S. Mordon, J. M. Devoisselle, S. Soulie-Begu, and T. Desmettre, "Indocyanine green: Physicochemical factors effecting its flourescence *in vivo*," *Microvasc. Res.*, vol. 55, pp. 146–152, 1998.

[22] S. Fickweiler, R. M. Szeimies, W. Baumler, P. Steinbach, S. Karrer, A. E. Goetz, C. Abels, F. Hofstadler, and M. Landthaler, "Indocyanine green: Intracellular uptake and phototherapeutic effects *in vitro*," *J. Photochem. Photobiol. B: Biology*, vol. 38, pp. 178–183, 1997.

[23] P. S. Tofts, DPhil, G. Brix, D. L. Buckley, J. L. Evelhoch, E. Henderson, M. V. Knopp, H. B. W. Larsson, T. Lee, N. A. Mayr, G. J. M. Parker, R. E. Port, J. Taylor, and R. M. Weisskoff, "Estimating kinetic parameters from dynamic contrast-enhanced T1-weighted MRI of a diffusable tracer: Standardized quantities and symbols," *J. Mag. Reson. Imag.*, vol. 10, pp. 223–232, 1999.

[24] P. S. Tofts, "Modeling tracer kinetics in dynamic Gd-DTPA MR imaging," *J. Magn. Reson. Imag.*, vol. 7, pp. 91–101, 1997.

[25] C. Chen, *Linear System Theory and Design*. New York: Oxford Univ. Press, 1999.

[26] P. Zarchan, *Fundamentals of Kalman Filtering: A Practical Approach*. Reston, VA: Amer. Inst. Aeronautics and Astronautics, 2000.

[27] C. K. Chui and G. Chen, *Kalman Filtering with Real Time Applications*. Berlin, Germany: Springer-Verlag, 1999.

[28] C. E. Catlin, *Estimation, Control, and the Discrete Kalman Filter*. New York: Springer, 1989.

[29] L. Ljung, "Asymptotic behavior of the extended Kalman filter as a parameter estimator for linear systems," *IEEE Trans. Automat. Control*, vol. AC-24, no. 1, pp. 36–50, Feb. 1979.

[30] R. Togneri and L. Deng, "Joint state and parameter estimation for a target-directed nonlinear dynamic system model," *IEEE Trans. Signal Process.*, vol. 51, no. 12, pp. 3061–3070, Dec. 2003.

[31] L. Nelson and E. Stear, "The simultaneous on-line estimation of parameters and states in linear systems," *IEEE Trans. Automat. Control*, vol. 21, no. 1, pp. 94–98, Feb. 1976.

[32] B. F. La Scala and R. R. Bitmead, "Design of an extended Kalman filter frequency tracer," *IEEE Trans. Signal Process.*, vol. 44, no. 3, pp. 739–742, Mar. 1996.

[33] M. Boutayeb, H. Rafaralahy, and M. Darouach, "Convergence analysis of the Extended Kalman Filter used as an observer for nonlinear deterministic discrete-time systems," *IEEE Trans. Automat. Control*, vol. 42, no. 4, pp. 581–586, Apr. 1997.

[34] B. J. Schnekenburger, "An extended Kalman filter as a parameter estimator for linear discrete time systems," masters thesis, New Jersey Inst. Technol., Newark, NJ, 1988.

[35] G. Schwarz, "Estimating the dimensions of a model," *Ann. Statist.*, vol. 6, pp. 461–464, 1978.

[36] G. E. P. Box, G. M. Jenkins, and G. C. Reinsel, *Time series analysis: Forecasting and control*, 3rd ed. Upper Saddle River, NJ: Prentice-Hall, 1994.

[37] H. Akaike, *Likelihood and the Bayes Procedure*, ser. Bayesian Statistics. Valencia, Spain: Univ. Press, 1980.

[38] A. Harvey, *Time Series Models*. Cambridge, MA: MIT Press, 1993.

[39] W. M. Sallas and D. A. Harville, "Noninformative Priors and Restricted Maximum Likelihood Estimation in the Kalman Filter," in *Bayesian Analysis of Time Series and Dynamic Models*, J. C. Spall, Ed. New York: Marcel-Dekker, Inc., 1988.

[40] F. Bevilacqua, A. J. Berger, A. E. Cerussi, D. Jakubowski, and B. J. Tromberg, "Broadband absorption spectroscopy in turbid media by combined frequency-domain and steady-state methods," *Appl. Opt.*, vol. 39, pp. 6498–6507, 2000.

[41] D. J. Jakubowski, *Development of Broadband Quantitative Tissue Optical Spectroscopy for the Non-Invasive Characterization of Breast Disease*. Irvine, CA: Beckman Laser Institute, Univ. California, 2002.

[42] S. Merritt, F. Bevilacqua, A. J. Durkin, D. J. Cuccia, R. Lanning, B. J. Tromberg, G. Gulsen, H. Yu, J. Wang, and O. Nalcioglu, "Monitoring tumor physiology using near-infrared spectroscopy and MRI coregistration," *Appl. Opt.*, vol. 42, pp. 2951–2959, 2003.

[43] L. M. Gray and L. D. Davisson, *An Introduction to Statistical Signal Processing*. Boston, MA: Cambridge Univ. Press, 2004.

[44] M. Y. Su, A. Muhler, X. Lao, and O. Nalcioglu, "Tumor characterization with dynamic contrast-enhanced MRI using MR contrast agents of various molecular weights," *Magn. Reson. Med.*, vol. 39, pp. 259–269, 1998.

[45] J. B. Fishkin, O. Coquoz, E. Anderson, M. Brenner, and B. J. Tromberg, "Frequency-domain photon migration measurements of normal and malignant tissue optical properties in a human subject," *Appl. Opt.*, vol. 36, pp. 10–20, 1997.

[46] D. L. Buckley, "Uncertainty in the analysis of tracer kinetics using dynamic contrast-enhanced T1-weighted MRI," *Magn. Reson. Med.*, vol. 47, pp. 601–606, 2002.

[47] A. Gelb, *Applied Optimal Estimation*. Cambridge, MA: M.I.T. Press, 1989.

[48] K. Licha, "Contrast agents for optical imaging," *Topics Curr. Chem.*, vol. 222, pp. 1–29, 2002.

[49] Y. Chen, G. Zheng, Z. Zhang, D. Blessington, M. Zhang, and H. Li, "Metabolism enhanced tumor localization by fluorescence imaging: *In vivo* animal studies," *Opt. Lett.*, vol. 28, pp. 2070–2072, 2003.

[50] R. Weissleder, C. H. Tung, U. Mahmood, and A. Bogdanov, "*In vivo* imaging with protease-activated near-infrared fluorescent probes," *Nat. Biotech.*, vol. 17, pp. 375–378, 1999.

Burak Alacam (S'99) received the M.S. degree in electrical, and computer engineering Department of Drexel University, Philadelphia, PA, in 2003. He is currently working towards the Ph.D. degree in the Electrical, Computer, and Systems Engineering Department of Rensselaer Polytechnic Institute, Troy, NY.

His research areas are biomedical signal and image processing, time series analysis, estimation and detection, inverse problems, and image reconstruction. His current research focuses on compartmental modeling of pharmacokinetics of fluorescence agents.

Birsen Yazici (S'92–M'93–SM'06) received the M.S. and Ph.D. degrees in mathematics and electrical engineering in 1990 and 1994, respectively, both from Purdue University, West Lafayette, IN.

From 1994 until 2000, she was a Research Scientist with the General Electric Company Research Center, Schenectady NY. During her tenure in industry, she worked on radar, industrial, and medical imaging systems. From January 2001 to 2003, she was with Drexel University Electrical and Computer Engineering Department, Philadelphia, PA. She joined the Electrical, Computer and Systems Engineering Department, Rensselaer Polytechnic Institute, in August 2003. Her research interests include inverse problems in medical imaging and radar, applied harmonic analysis, X-ray imaging, diffuse optical tomography, biomedical optics, synthetic aperture radar, and waveform design. She holds 12 patents.

Xavier Intes received the Ph.D. degree in physics from the University of Bretagne Occidentale,Brest, France, in 1998.

He joined Prof. Chance's laboratory in 1999 as a Postdoctoral Fellow at the University of Pennsylvania, Philadelphia. In 2001, he acted as the Director of Research of the Medical Diagnostic Research Foundation, and the Director of Research of Optical Devices Inc., Philadelphia. In 2003, he joined Advanced Research Technologies Inc., Saint-Laurent, QC, Canada, as a Senior Staff Scientist and later acted as ART's Chief Scientist. His research is focused on application of optical techniques for biomedical imaging of small animal and in clinical settings.

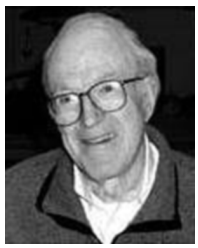

Britton Chance received the Ph.D. degree in chemistry from the University of Pennsylvania, Philadelphia, in 1940 and the Ph.D. degree in biology from Cambridge University, Cambridge, U.K., in 1942. He received the D.Sc. degree from Cambridge University in 1952.

He is Eldridge Reeves Johnson University Professor Emeritus of Biochemistry and Biophysics and Physical Chemistry and Radiologic Physics, School of Medicine, University of Pennsylvania, Philadelphia, and President, Medical Diagnostic Research Foundation (MDRF), Philadelphia.